Waterborne Polyurethane/Clay Nanocomposites: Novel Effects of the Clay and Its Interlayer Ions on the Morphology and Physical and Electrical Properties

Hsun-Tsing Lee* and Li-Huei Lin

Department of Chemical and Materials Engineering, Vanung University, Chung-Li 320, Taiwan, ROC

Received March 20, 2006; Revised Manuscript Received June 14, 2006

ABSTRACT: A modified clay was used to prepare waterborne polyurethane (WPU)/clay nanocomposite dispersions in this study. XRD and TEM examinations indicate that the clay platelets are exfoliated. Moreover, AFM phase image of the WPU/clay film shows that the isolated clay-rich phases are surrounded by a continuous WPU-rich phase. Clay does not influence the location and peak broadness of the T_g of soft segment domains in the WPU/clay films. However, clay raises the T_g of hard segment domains, which is probably due to the ionic interactions between the clay and hard segments of WPU. These ionic interactions could be evidenced by IR spectra of the WPU/clay nanocomposites. The WPU/clay dispersion with higher clay content exhibits a larger average particle size, a less negative zeta potential, and a higher viscosity, whereas the corresponding cast film possesses lower volumetric and surface electrical resistances. The volumetric and surface electrical resistances of the WPU/clay nanocomposite film are nearly identical. This indicates that clay platelets do not migrate to the surface regions of WPU/clay films because of the above-mentioned ionic interactions. In addition, the incorporation of clay is also capable of enhancing the thermal resistance and tensile properties of WPUs dramatically.

Introduction

Polyurethanes (PUs) are functional polymers whose properties can be tailor-made by simply adjusting the compositions. Because of this, the PUs are of great interest for applications in coatings, adhesives, medical devices, binders, sealants, and textiles industries.[1−5] Conventional polyurethane products such as coatings and adhesives contain a significant amount of organic solvents and sometimes even free isocyanate monomers.[6] Therefore, these solvent-based polyurethanes have been gradually replaced by the waterborne polyurethanes (WPUs) because of the increasing concern about environmental pollution and health and safety risks.

The performance of solvent-based and waterborne polyurethanes can be enhanced by incorporating nanosized layered silicates. Recently, montmorillonite (MMT), a layered silicate with lamellar shape, has attracted intensive research interest for the preparation of polymer/clay nanocomposites. This is because the lamellar platelets of MMT display high in-plane strength, stiffness, and high aspect ratio.[7] Typically, the chemical structure of MMT consists of two fused silica tetrahedral sheets sandwiching an edge-shared octahedral sheet of either magnesium or aluminum hydroxide. The Na^+ and Ca^{2+} residing in the interlayer galleries can be replaced by organic cations such as alkylammonium ions via a cationic-exchange reaction to render the hydrophilic layered silicate organophilic. According to several recent works, the incorporation of nanolayers of mineral clay was found to enhance the thermal stability,[8−12] mechanical strength,[13−18] molecular barrier,[19−21] and elasticity[22−25] properties of the solvent-based polyurethanes. Moreover, the morphology of the solvent-based polyurethane/clay nanocomposites was also examined.[26−28]

In literature mentioned previously, most of the polyurethane/clay nanocomposites were prepared in various organic solvents, whereby plenty of organic solvent needs to be removed. In fact, the polyurethane moieties of these nanocomposites are solvent-based. Only a few waterborne polyurethane/clay nanocomposites were reported in the literature, which were prepared either by a modified acetone process[29] or by a physical blending way.[30] In the modified acetone process, there was still plenty of organic solvent used. The removal of volatile solvent would increase the number of preparation steps and degree of inconvenience to obtain the final product. On the other hand, the blending method is simply by mixing PU latex with aqueous silicate dispersion. This results in a latex while organic PU moieties and hydrophilic silicate particles locate in different phases. In this work, a prepolymer mixing process, one of the methodologies for preparating WPUs,[31] was adopted to avoid the use of a large amount of organic solvent. The as-synthesized aqueous PU/clay nanocomposite dispersions can be used directly and nonhazardously. In addition, the hydrophobic organoclay of the product would locate in the inner parts of PU particles, which differs from the morphology of the product obtained by the blending method. It is important to note that the WPU/clay nanocomposites prepared through the prepolymer mixing process were rarely reported.[32] Moreover, the nanocomposites prepared from different synthesis processes and/or raw materials would be expected to exhibit different characteristics and properties.

Apart from that, the MMT clay possesses a structure consisting of extended anionic layers balanced by mobile interlayer cations.[33] The interlayer ions would expose themselves outward to the ionic WPU as the clay was exfoliated by WPU. To our best knowledge, there is no information in the literature about the study of ionic interactions between the clay and WPU. An investigation of the ionic interaction effects is of prime importance for the illustration and utilization of these ionic WPU/clay nanocomposites. Herein, the effects of clay and interlayer ions on the morphology, physical properties, glass transition, and ionic conductivities of the WPU/clay nanocomposites prepared by the prepolymer mixing process are reported.

Experimental Section

Materials. Isophorone diisocyanate (IPDI), dimethylolpropionic acid (DMPA), and dibutyltin dilaurate (T-12) were purchased from

* Corresponding author.

10.1021/ma060621y CCC: $33.50
Published on Web 08/03/2006

Lancaster. *N*-Methyl-2-pyrrolidone (NMP) was obtained from Ferak. Triethylamine (TEA) and ethylenediamine (EDA) were obtained from Tedia. Didodecyldimethylammonium bromide (DMAB), $[CH_3(CH_2)_{11}]_2(CH_3)_2NBr$, was purchased from Aldrich. All reagents and solvent were synthetic grade and used as received. Poly(hexylene adipate)diol with an average molecular weight of 1900 was obtained from Yong Shun Chemical Co., Taiwan, and is designated as PHAO. The PHAO polyols were dried and degassed at 100 °C under dynamic vacuum at 3−5 mmHg for 4 h. The montmorillonite (MMT) clay (designated as PK802) was supplied by Paikong Ceramic Materials Co., Taiwan.

Preparation of Organophilic Clay. MMT (PK802) is a hydrophilic clay containing stacked silicate sheets that can exchange cations with quaternary ammonium cations.[34] Through this cation-exchange reaction, the long alkyl chains of quaternary ammonium cation can be intercalated into the MMT clay galleries and enlarge the spacing between the layers. Both the enlarged spacing and organophilic nature of the alkyl chains in ammonium cations would facilitate the intercalation of polymer chains or organic monomers into the clay. Therefore, the clay becomes organophilic after the cation-exchange reaction.

During the cation-exchange reaction, MMT (5 g) was gradually added to an aqueous solution of DMAB or intercalating agent at room temperature and stirred for 12 h. The equation for calculating the intercalating agent needed for a cation-exchange reaction is

$$95/100 \times 5\ \text{g (for clay)} \times 1.2 = (X/M_w \text{ of intercalating agent}) \times 1 \times 1000$$

where X represents the amount of intercalating agent used, 95/100 represents the cationic exchange capacity (CEC) of 95 mequiv per 100 g of MMT clay, and 1.2 (>1) indicates the excess amount of intercalating agent used. After the cation-exchange reaction, the obtained modified clay was washed repeatedly with deionized water until no AgCl precipitates were found while the filtrate was titrated with 0.1 N $AgNO_3$ solution continuously. The wet modified clay was dried at 100 °C for 12 h. The dried modified clay was ground to powdery state and screened with a 325 mesh sieve.

Preparation of WPU/Clay Nanocomposite Dispersions. A 500 mL four-neck glass flask equipped with a heating mantel, a mechanical stirrer, a thermometer, a reflux condenser, and a nitrogen atmosphere was used as reactor. The IPDI and modified clay were mixed in a sealed bottle and stirred at room temperature overnight to become an IPDI/clay hybrid. Then aqueous WPU/clay dispersions were prepared by the prepolymer mixing process, as shown in Scheme 1. The formulations used are shown in Table 1. The PHAO, DMPA, NMP, and a few drops of T-12 catalyst were added to the reactor, and the reaction mixture was heated to 75 °C. Subsequently, IPDI/clay hybrid was slowly added to the reactor while the reaction temperature remained at 75 °C. The reaction proceeded until the amount of residual isocyanate groups reached a theoretical end point, which was calculated as all hydroxyl groups had reacted with the isocyanate groups. The NCO content of the prepolymer was measured by the dibutylamine back-titration method.[35] An NCO-terminated prepolymer was therefore obtained. The prepolymer was cooled to 50 °C, whereas triethylamine was added to neutralize the COOH groups of DMPA. The obtained polyurethane/clay anionomer was then dispersed in water and chain extended by reacting with ethylenediamine to become an aqueous polyurethane/clay nanocomposite dispersion with a solid content of 25 wt %. A WPU/clay nanocomposite film can be obtained by drying the dispersion at 60 °C in a Teflon trough for 4 days and then under dynamic vacuum at 60 °C for 24 h.

Characterization. An X-ray diffractometer (XRD, Thermo model ARL X'TRA) was used to examine ordering in clay and WPU/clay nanocomposites. The X-ray beam was Ni-filtered Cu Kα radiation from a sealed tube operated at 45 kV and 40 mA. Data were obtained in the 2θ range of 0.5°−30° at a scan rate of 1.8°/min.

A transmission electron microscope (TEM, Hitachi model H-7500) was used to examine the morphology of the WPU/clay

Scheme 1. Schematic Representation of the WPU/Clay Nanocomposite Preparation Process

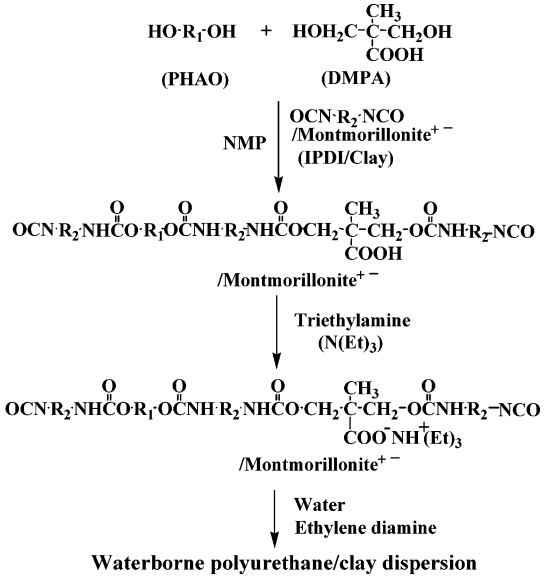

where

$R_1 =$ 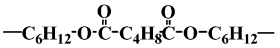

$R_2 =$ 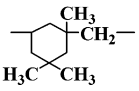

nanocomposites. The samples for TEM examination were first prepared by placing the nanocomposite films into epoxy capsules and curing the epoxy at 70 °C for 24 h in an oven. The cured epoxies containing WPU/clay nanocomposites were then microtomed with a diamond knife into 70−90 nm thick slices at −100 °C. Finally, a 3 nm thick carbon layer was deposited on these slices that were on 200 mesh copper nets for TEM observation.

Atomic force microscopy (AFM) scans were performed using a CP II instrument from Digital Instruments. Generally, there are two kinds of imaging modes, i.e., tapping and contact modes. Tapping mode was used in this study that the oscillating probe cantilever causes the tip to make only intermittent contact with the sample. With respect to the phase of the sine wave driving the cantilever, the phase of tip oscillation is quite sensitive to various sample surface characteristics. Therefore, the tip can also sense the phase images of the sample surface in addition to the topography. The specimens were cut from the WPU/clay nanocomposite films with different clay contents.

A Fourier transform infrared spectrophotometer (FTIR; Perkin-Elmer model Spectrum one) was used to identify the chemical structure of waterborne polyurethane/clay nanocomposites. The dispersion sample was coated as a thin liquid film on thallium bromide/thallium iodide crystal surface and dried for examination. The thallium bromide/thallium iodide crystal is water-insensitive.

A particle sizer (Microtrac model S3000) was used to measure the particle diameter distributions and their average diameters of the WPU/clay dispersions under dynamic circulation.

A coaxial cylinder rheometer (Brookfield model DV III+) equipped with a thermostat was used to measure the viscosities of the aqueous WPU/clay dispersions at 25 °C. The viscosities of dispersion samples were measured as a function of shear rates from 1.2 to 305.8 1/s. However, steady viscosities at a shear rate of 2.5 1/s were used to evaluate the viscosity variations of WPU/clay dispersions with different clay contents. A 16 mL dispersion sample with a solid content of 25 wt % was tested every time.

A zeta potential analyzer (Malvern model Zetasizer 3000) was used to measure the zeta potentials of the aqueous WPU/clay

Table 1. Formulation of the Waterborne Polyurethane/Clay Dispersions[a]

	weight of raw materials (g)							
clay content (wt %)[b]	IPDI	clay	PHAO	DMPA	NMP[c]	TEA[d]	H_2O[e]	EDA
0	25.0	0	60.3	4.13	22.4	3.3	255.0	3.0
1	25.0	0.93	60.3	4.13	22.6	3.3	257.5	3.0
2	25.0	1.86	60.3	4.13	22.9	3.3	260.0	3.0
3	25.0	2.79	60.3	4.13	23.1	3.3	263.0	3.0
4	25.0	3.72	60.3	4.13	23.3	3.3	265.2	3.0
5	25.0	4.65	60.3	4.13	23.6	3.3	268.0	3.0

[a] NCO/OH molar ratio = 1.8. [b] Based on nonvolatile parts of the dispersion, i.e., with NMP, TEA, and H_2O excluded. [c] NMP content is about 6.0 wt % of the dispersion. [d] Moles of TEA equal to those of DMPA. [e] Appropriate amount of water is added to form a dispersion of solid content 25 wt %.

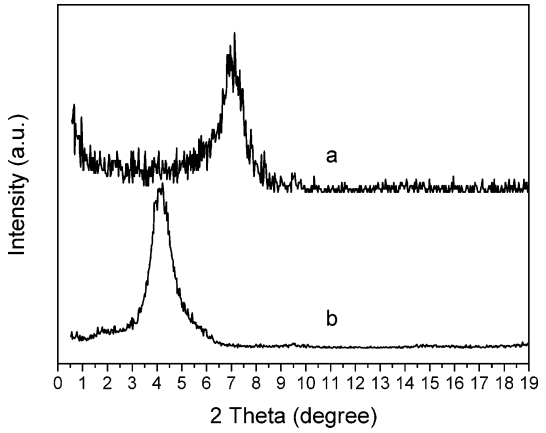

Figure 1. X-ray diffraction patterns of the PK802 clay before (a) and after (b) modification with DMAB.

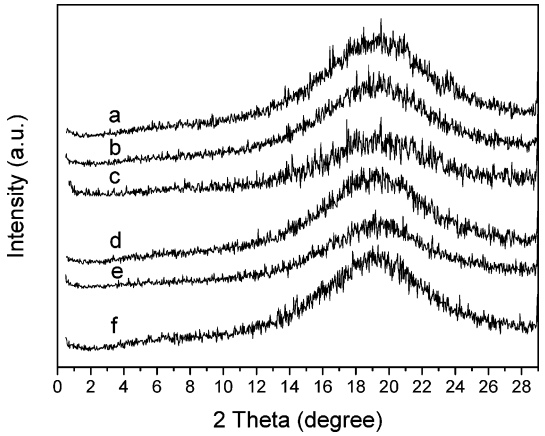

Figure 2. X-ray diffraction patterns of the WPU/clay nanocomposites with different clay contents: (a) 0, (b) 1, (c) 2, (d) 3, (e) 4, and (f) 5 wt %.

dispersions at 25 °C. The dispersions were diluted with deionized water to 0.5 wt % before measurement.

A thermogravimetric analyzer (TGA; Perkin-Elmer model TGA-7) was used to measure weight losses of the WPU/clay films in the temperature range 40−500 °C with a heating rate of 10 °C/min and under a nitrogen stream. Prior to the temperature scan, each specimen was subject to a heating scan from room temperature to 100 °C in the TGA furnace to remove any adsorbed moisture.

A dynamic mechanical analyzer (DMA; TA model Q800) was used to measure the flexural, loss moduli (E', E''), and tan δ of WPU/clay films in the temperature range −140 to +100 °C with a heating rate of 2 °C/min and frequency of 1 Hz. The size of the specimens was about 20 mm long, 5 mm wide, and 0.3 mm thick. After mounting a specimen in the sample chamber, the specimen length subjected to cyclic flexural motion was about 15 mm.

Uniaxial stress−strain testing was performed using a Shimadzu model EZ Test machine at room temperature with a crosshead speed of 20 mm/min. Dumbbell-shaped samples were stamped out of cast films with a standard ASTM D1708 die.

An electrical resistance meter (Monroe Electronics model 272A) was used to measure the surface and volumetric electrical resistances of WPU/clay films at room temperature. The size of the specimens was about 68 mm in diameter and 0.3 mm in thickness.

Results and Discussion

Morphology and Structure of the WPU/Clay Nanocomposites. Before and after modification with DMAB salt, the PK802 clay exhibits XRD diffraction peaks at $2\theta = 7.1°$ and 4.2°, respectively (Figure 1). The interlayer spacings calculated from the above two peaks using the equation $2d \sin \theta = n\lambda$ are 1.24 and 2.10 nm, respectively. The DMAB enlarges the interlayer spacing of PK802 clay dramatically. Moreover, the hydrophilic pristine clay becomes organophilic due to the presence of alkylammonium cations in the interlayer galleries. The organoclay is thus compatible with urethane monomers and applicable in subsequent synthesis of WPU/clay nanocomposites.

X-ray diffraction analyses of the WPU/clay nanocomposites with different clay contents are shown in Figure 2. Each WPU/clay nanocomposite exhibits a broad diffraction halo at $2\theta = 19°$, which is the same as that of the pure WPU. This diffraction halo is associated with the amorphous phase of WPU. The characteristic diffraction peak at $2\theta = 4.2°$ observed previously for the modified PK802 clay disappears, suggesting that the clay platelets are exfoliated. The composite with as high as 5 wt % clay can still achieve completely exfoliated silicate platelets. For many solvent-based PU/clay nanocomposites with the absence of ions in PU moieties, the electrostatic forces between the clay platelets would have a tendency to squeeze the PU polymer chains out and subsequently result in an intercalated structure.[8,19−21,26,36] The clay intercalated with the PU polymer would exhibit a reflection at $2\theta = 2.5°$ for a certain solvent-based PU/clay nanocomposite.[21] In the WPU/clay system studied in this work, the above-mentioned squeeze effect was overcome by the ionic attractions between anionic WPUs and cationic clay platelets. Therefore, the intercalated WPU polymer chains could peel the platelets away from the well-intercalated silicate stacks or tactoids, resulting in an exfoliated silicate system.

Figure 3 shows the TEM micrograph of the cross section of a WPU/clay nanocomposite with 5 wt % clay. The dark lines are intersections of clay sheets. The TEM micrograph proves that clay platelets are exfoliated in the WPU polymer matrix. No reflection of parallel silicate stacks observed in the X-ray diffractogram corresponds to the fact of randomly oriented exfoliated platelets seen in the TEM micrograph. Nevertheless, it is important to note that the X-ray diffraction analysis gives macroscopic information, while TEM photograph gives local microscopic information only.

AFM is another useful technique for the morphology examination. Using tapping mode, AFM can map the topographic features as well as the phase characteristics on a surface. The phase image often not only reveals features that are invisible

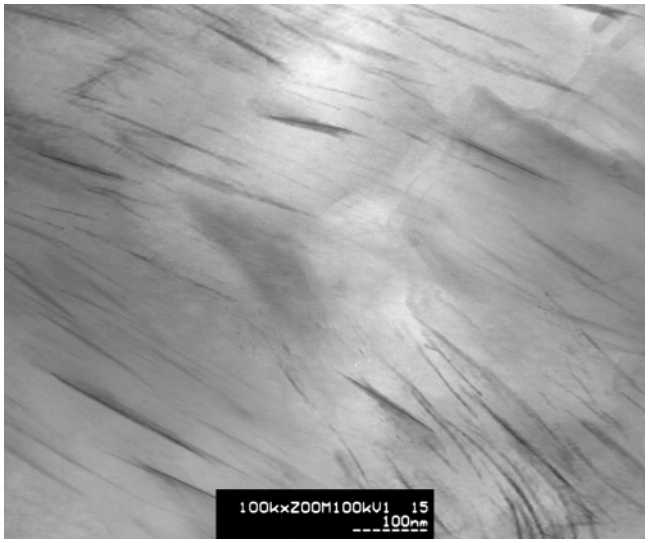

Figure 3. TEM microphotograph of the WPU/clay nanocomposite with 5 wt % clay.

topographically but also can render these characteristics in higher resolution and/or signal-to-noise-ratio (SNR) than those produced by the roughness data. Phase imaging detects the phase shift associated with the probe's resonance and its proximal interaction with the sample. Phase imaging is very effective in mapping the submicron morphology of multicomponent polymer composites based on the relative elasticity of individual components.[27]

Figure 4 shows the AFM topographic and phase images of the WPU/clay nanocomposite films containing 0, 1, and 5 wt % clay. The appearances of topographic and phase images of the pure WPU film are similar. Both images show continuous global domains with some bumpy areas. Owing to the absence of clay, the phase image of the WPU film is affected by roughness data and shows mainly the surface topography. However, these two kinds of images of WPU/clay films with higher clay content become less similar. Despite that both topographic and phase images of the WPU/clay film containing 1 wt % clay show rugged domains or phases, the appearances of these two images are somewhat dissimilar. The topographic and phase images of the pristine WPU are strongly influenced by the incorporation of 1 wt % clay. The WPU/clay nanocomposite film with 5 wt % clay shows quite disparate features between the topographic and phase images. The topographic image looks lumpy, while the phase image is filled with isolated small domains of irregular granular or channel-like shapes. In the phase image, the continuous brighter domain is the WPU-rich phase and the isolated darker domains are clay-rich phases because WPU is the major moiety of this nanocomposite. This phase image of the WPU/clay film with 5 wt % clay indicates that most clay-rich phases are nanosized, and aggregation does occur sparsely.

IR spectra of the WPU/clay films with clay contents of 0, 1, 3, and 5 wt % are shown in Figure 5. The WPU possesses basic functional groups of urethane and ester because of the polyester diol structure of PHAO. The 2949 and 2867 cm^{-1} peaks are due to the alkane $-CH$ stretching vibration. The 1733 and 1656 cm^{-1} peaks are due to the free and ion-interacted $C{=}O$ stretchings, respectively. The occurrence of this ion-interacted $C{=}O$ stretching is due to the ionic interactions between $-COO^-$ ions of neutralized DMPA and quaternary ammonium cations of clay that is discussed afterward. The other characteristic peaks are 1557 cm^{-1} due to the CHN vibration of associated secondary urethane groups, 1462 cm^{-1} due to CH_2 and CH_3 deformation vibrations, 1386 and 1364 cm^{-1} due to the $C-N$ stretching, 1241 cm^{-1} due to the ester $C-O-C$ asymmetric stretching vibration, 1174 cm^{-1} due to the coupled $C-N$ and $C-O$ stretching vibrations, and 1062 cm^{-1} due to the ester $C-O-C$ symmetric stretching vibration.[37] The $Si-O$ stretching vibration of clay, supposedly located at 1046 cm^{-1},[36] is too weak and overlapped with the above-mentioned 1062 cm^{-1} absorption peak. These IR spectra confirm the formation of a polyurethane structure. Moreover, no peak of free NCO group at 2250−2285 cm^{-1} was observed in these spectra. Therefore, the NCO-terminated prepolymer was fully reacted with ethylenediamine during the synthesis process.

DMPA is a small molecular diol containing a hydrophilic COOH group. This COOH group could be neutralized to $-COO^-NH^+(C_2H_5)_3$ salt by triethylamine during synthesis of a WPU/clay dispersion. The WPU/clay dispersions are electrostatically stabilized with $-COO^-$ ions of neutralized DMPA, while their counterions $NH^+(C_2H_5)_3$ locate in the neighborhood. Therefore, ionic interactions between these two kinds of ions would be present in the WPU dispersion. Moreover, the modified clay has a structure consisting of extended anionic layers balanced by quaternary ammonium cations in the interlayer galleries. When the clay was exfoliated by WPU polymer chains, the cations and anions of clay would interact with $-COO^-$ and $NH^+(C_2H_5)_3$ ions of WPU, respectively. After casting the WPU/clay dispersion into a film, these ions would contribute ionic conductivity to the film. This will be discussed in a later section. Because of these ionic interactions, IR spectra of WPU/clay composites exhibit free and ion-interacted $C{=}O$ stretching peaks at 1733 and 1656 cm^{-1}, respectively. The absorbance ratio of the $C{=}O$ stretching peak at 1656 cm^{-1} to that at 1733 cm^{-1} was designated as Ar. The Ar values of WPU/clay composites with clay contents of 1 and 5 wt % are 0.28 and 0.38, respectively (Figure 5). The Ar increases with increasing clay content. Therefore, there are more ion-interacted $C{=}O$ groups for the WPU/clay with higher content of clay. Because DMPA constitutes partial hard segments of WPU, it is concluded that IR spectra of WPU/clay nanocomposites show the presence of strong ionic interactions between the clay and hard segments of WPU.

Physical Characteristics and Zeta Potentials of the WPU/Clay Dispersions. The WPU/clay dispersions show no precipitates or unstable aggregates. The particle size distributions of the WPU/clay dispersions with different clay contents are shown in Figure 6. The pure WPU dispersion exhibits unimodal distribution, whereas the composite dispersions exhibit multimodal distributions. Moreover, the particle size distribution of the composite dispersion becomes broader and shifts to larger particle sizes with increasing clay content. The calculated volumetric average particle diameters of the dispersions with different clay contents are shown in Figure 7. The average particle diameter of the WPU dispersion is 49 nm, which is nanosized. The average particle diameters of the WPU/clay dispersions with clay contents of 1 and 5 wt % are 58 and 138 nm, respectively. One reason for the increase of average particle diameter with increasing clay content is probably due to the hydrophobic nature of alkyl groups of the modified clay. Meanwhile, this increase also could possibly result from the ionic interactions between WPU and clay. The WPU dispersion is electrostatically stabilized by $-COO^-$ ions of neutralized DMPA. Therefore, a stable electrical double layer is formed around each WPU particle. The cations of exfoliated clay platelets would interact with $-COO^-$ ions and interfere with

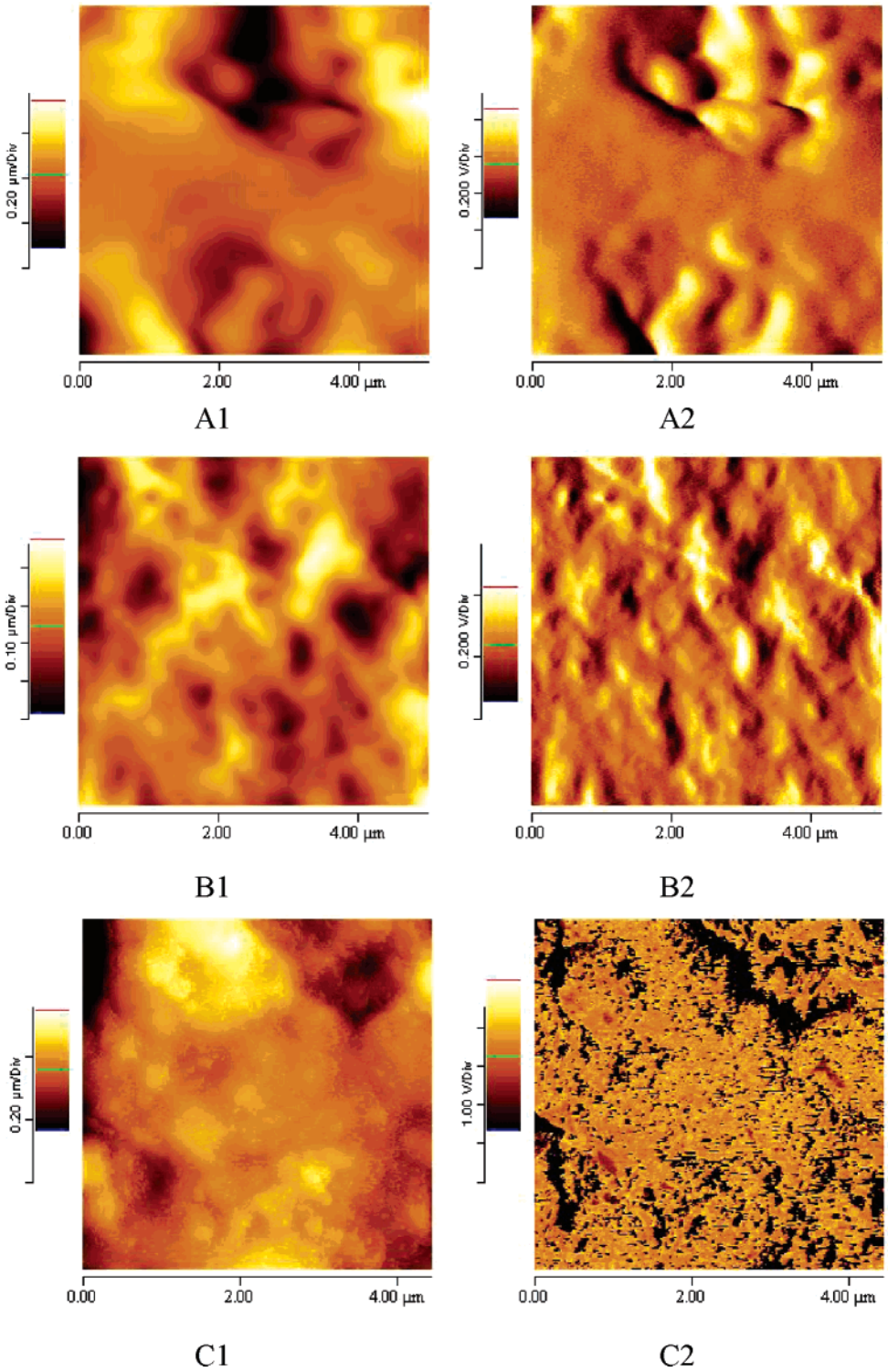

Figure 4. AFM topographic and phase images of the WPU/clay nanocomposites with different clay contents. Clay content: A, 0 wt %; B, 1 wt %; C, 5 wt %. Topography: A1, B1, C1. Phase: A2, B2, C2.

the double layer of pristine WPU dispersion. The WPU/clay dispersion disturbed by ionic clay platelets would have less effective hydrophilic groups for being stabilized in water. This would lead to a larger average particle size. The fact that WPU/clay dispersion is less stable than pristine WPU dispersion is also indicated by the less negative zeta potential of the former in Figure 8 and related discussion afterward.

Figure 7 also shows the viscosities of the WPU/clay dispersions with different clay contents at 25 °C. All these dispersions have a fixed solid content of 25 wt %. The viscosity of the WPU dispersion is 5 cps, which is not viscous. The viscosities of WPU/clay dispersions with clay contents of 1 and 5 wt % are 6 and 72 cps, respectively. The increase of viscosity with increasing clay content is probably due to the presence of more clay ions in every WPU/clay particles. The stronger electrostatic interactions among larger quantities of ions would promote the viscosities of WPU/clay dispersions.

Figure 8 shows the zeta potentials of the WPU/clay dispersions with different clay contents. The anionic WPU particles of the WPU dispersion are stabilized in water by COO^- ions of neutralized DMPA. Consequently, the particles would exhibit negative surface charges and zeta potentials. The WPU disper-

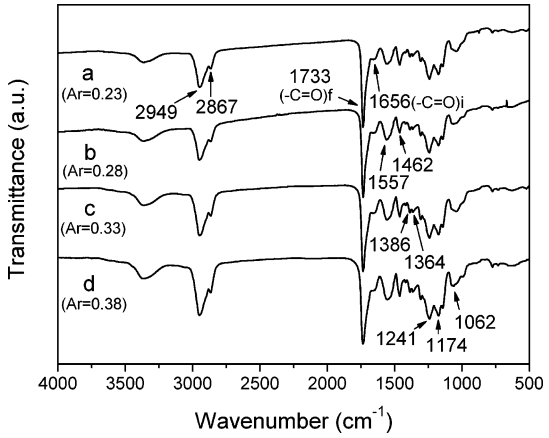

Figure 5. IR spectra of the WPU/clay nanocomposites with different clay contents: (a) 0, (b) 1, (c) 3, and (d) 5 wt % (Ar represents the absorbance ratio of ion-interacted C═O peak at 1656 cm^{-1} to free C═O peak at 1733 cm^{-1}).

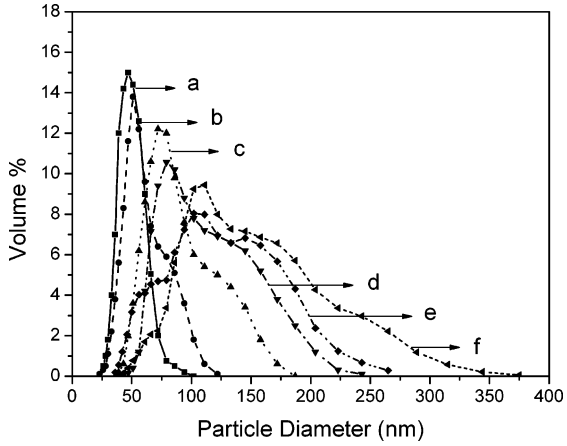

Figure 6. Particle size distributions of the WPU/clay nanocomposites with different clay contents: (a) 0, (b) 1, (c) 2, (d) 3, (e) 4, and (f) 5 wt %.

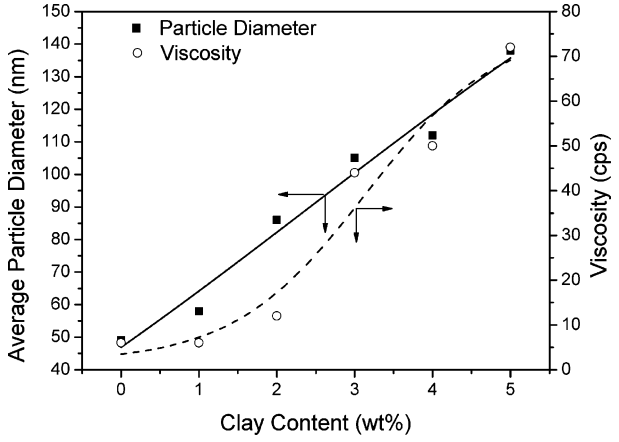

Figure 7. Volumetric average particle diameters and viscosities of the WPU/clay dispersions with different clay contents. The symbols are experimental data, and curves are the curve-fitting results in this and following figures.

sion has a negative zeta potential of −48.1 mV. The alkylammonium cations of exfoliated clay platelets would interact with the COO^- ions and diminish the stabilizing effect of the latter ions in the WPU/clay dispersion. Therefore, it would make the zeta potential of the WPU/clay dispersion less negative than that of the pristine WPU dispersion. The zeta potentials of WPU/clay dispersions with clay contents of 1 and 5 wt % are −41.2 and −26.7 mV, respectively. The WPU/clay dispersion with less negative zeta potential would be less stable and possess larger average particle size, as shown in Figure 7.

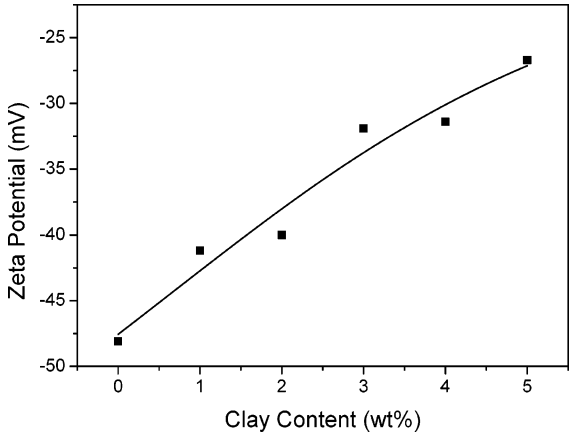

Figure 8. Zeta potentials of the WPU/clay dispersions with different clay contents.

Considering a spherical particle with a radius **R**, carrying a charge **q** in a medium of dielectric constant ϵ, electrostatic theory gives the potential of the particle as $\mathbf{q}/\epsilon\mathbf{R}$. If the charge is in the diffuse double layer only, then the potential is zeta potential ξ, and since the thickness of the Helmholtz double layer is negligible compared with the radius of particles, **R** may be put equal to the radius of the particle plus its Helmholtz layer. Hence[38]

$$\xi = \mathbf{q}/\epsilon\mathbf{R}$$

A WPU/clay particle with a higher content of clay would exhibit larger **R** (Figure 7). Moreover, there is less effective negative charge **q** present in the double layer due to the interactions of COO^- ions with clay platelet cations. This would lead to a less negative ξ, as shown in Figure 8. Therefore, the phenomenon that the WPU/clay dispersion with higher clay content exhibits a less negative zeta potential could also be explained by using the equation $\xi = \mathbf{q}/\epsilon\mathbf{R}$.

Thermal and Mechanical Properties of the WPU/Clay Films. Figure 9 shows the results of TGA measurements for the WPU/clay films with different clay contents. The insert in Figure 9B shows the partial TGA results for better discernment of weight losses before 250 °C. The weight losses at 210 °C are listed in Table 2, while the specific values of the WPU/clay films with clay contents of 0 and 5 wt % are 1.0 and 2.1 wt %, respectively. The weight loss of the WPU/clay film increases with increasing clay content before 220 °C. This is due to the presence of organic alkylammonium compound used for clay modification. However, after the complete decomposition of the small organic molecules, the WPU/clay film containing more clay exhibits higher thermal resistance. This enhancement of thermal resistance by the presence of clay can be found when heating the WPU/clay film above 250 °C. As shown in Table 2, the weight losses of the WPU/clay films at 320 °C with clay contents of 0 and 5 wt % are 31.6 and 19.1 wt %, respectively. The WPU/clay film containing more clay exhibits higher thermal resistance because of the high thermal insulation effect of clay. The WPU moiety is almost completely decomposed above 450 °C. It is obviously that the WPU/clay film with higher clay content exhibits weightier residue at 500 °C.

DMA results of the WPU/clay nanocomposite films with different clay contents are shown in Figure 10. From E'' curves, three transitions, β, α, and α', are observed, and their characteristic peaks are listed in Table 2. The insert in Figure 10B

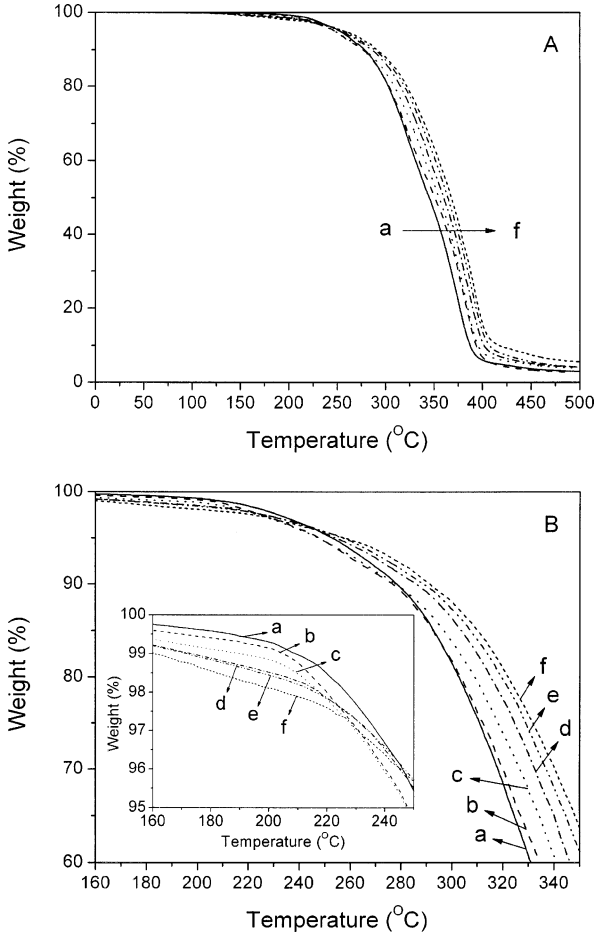

Figure 9. TGA curves of the WPU/clay films with different clay contents: (a) 0, (b) 1, (c) 2, (d) 3, (e) 4, and (f) 5 wt %.

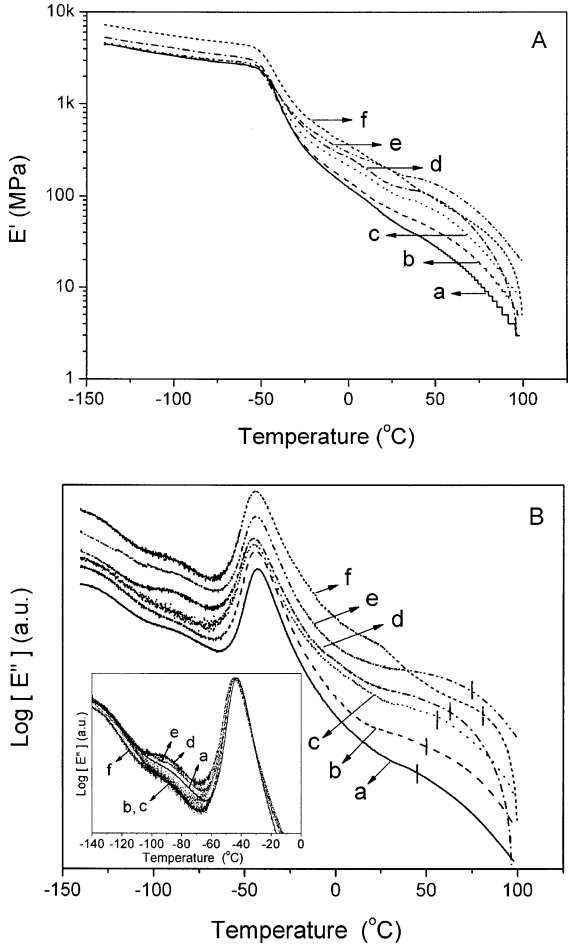

Figure 10. DMA results of the WPU/clay films with different clay contents: (a) 0, (b) 1, (c) 2, (d) 3, (e) 4, and (f) 5 wt %.

Table 2. Weight Losses and Transition Temperatures of the WPU/Clay Nanocomposite Films from TGA and DMA Analyses

clay content (wt %)	weight loss (%)		transition temp (°C)		
	210 °C	320 °C	β	α	α¢
0	1.0	31.6	−85	−43	45
1	1.2	30.1	−87	−44	50
2	1.5	26.1	invisible	−44	56
3	1.7	22.4	−90	−44	63
4	1.8	20.3	−90	−45	75
5	2.1	19.1	−87	−44	81

shows the α transition peaks that are shifted in the *y*-axis direction for the comparison of peak broadness. The second transition temperature (T_α, centered in the range of −45 to −43 °C) can be assigned as the glass transition temperature of the soft segment domains (T_g-S) because E' drops by 1−2 orders in the transition region. The location of T_g-S in the DMA spectra is nearly irrespective of the clay content. As the temperature increases beyond the transition region of T_g-S, E' changes from a rapid decrease to a slow decrease and then to a rapid decrease again. On the other hand, E'' also exhibits similar changes and generates a shoulder with an onset point in the range of 45−81 °C, which is marked by a short bar on each curve. This transition at the high-temperature range is designated as α' transition. The α' transition is the glass transition of hard segment domains which would become more pronounced and at higher temperature (T_g-H) with increasing clay content. For the WPU/clay films with clay contents of 3−5 wt %, α' transitions are overlaid by viscous flows indicated by the rapid decrease of E' values during the transition ranges. Viscous flow would occur when a large fraction of the entanglements of polymer chains move so as to relieve the stress upon them during measurement.

For some reports on solvent-based PU/clay nanocomposites with PU chains intercalated in the clay galleries,[17,39] the T_g-S shifted to higher temperature with increasing clay content because of the confinement of PU chains by the clay. Moreover, the T_g-S peaks of these solvent-based PU/clay nanocomposites were broadened due to the motion of polymer chains at the polymer−clay matrix interface.[17] The T_g-S shifting and peak broadening of nonionic solvent-based PU by the presence of clay indicated the intercalation of PU chains in the clay galleries. In our WPU/clay nanocomposites, the clay content does not influence the location and peak broadness of the T_g-S, as shown in Figure 10B, indicating that WPU chains are not confined by the clay. Thus, clay platelets are exfoliated in our WPU/clay nanocomposites as was also confirmed by the XRD and TEM measurements previously. Moreover, the clay enhances the presence of glass transition of the hard segment domains and further raises the transition temperature. This is probably due to the ionic interactions between the ionic hard segments of WPU and clay platelets. The clay also enhances the phase separation degree of the soft and hard segment domains of the WPU component because the WPU/clay film containing more clay exhibits a greater difference between T_g-S and T_g-H. In the β transition region at the low-temperature range, E'' exhibits a small broad peak centered in the range of −90 to −85 °C, whereas E' drops by less than 0.1 order in magnitude. This transition may be attributed to a special twisting or librational motion of short segments of methylene units in a trans

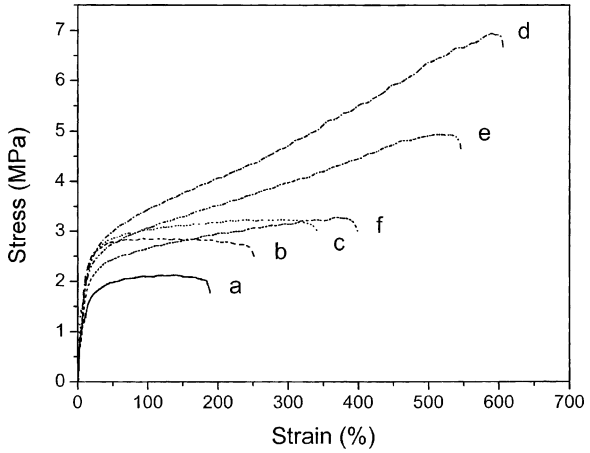

Figure 11. Stress−strain curves for the WPU/clay films with different clay contents: (a) 0, (b) 1, (c) 2, (d) 3, (e) 4, and (f) 5 wt %.

Table 3. Tensile Properties of the WPU/Clay Nanocomposite Films with Different Clay Contents

clay content (wt %)	tensile strength (MPa)	elongation at break (%)
0	2.12	189
1	2.86	252
2	3.24	343
3	6.93	606
4	4.94	546
5	3.28	398

configuration of the PHAO.[40,41] This motion requires some deformation of bond angles.[40]

Stress−strain curves for the WPU/clay films with different clay contents are shown in Figure 11. The corresponding tensile properties are summarized in Table 3. The clay content has a profound effect on the tensile properties. It is evident that even the presence of a small amount of clay would largely improve the tensile properties. For the WPU/clay composite containing 1 wt % clay, tensile strength and elongation at break are about 35% and 33%, respectively, higher than those for the pristine WPU sample. In contrast to the conventional filled polymer systems, the increase in strength does not come at the expense of the ductility. Both the tensile strength and elongation at break of the WPU/clay composites increase with increasing clay content in the range of 0−3 wt %. The maximum tensile properties are reached for the sample with 3 wt % clay. Both the tensile strength and elongation at break for the WPU/clay composite with 3 wt % clay are more than 3 times higher than those for the pristine WPU sample. When the clay content is higher than 3 wt %, the tensile properties of the WPU/clay composite decrease slightly. This is probably due to some degree of aggregation of the exfoliated clay platelets as shown in the previous AFM phase images. Generally, both the tensile strengths and elongations at break are enhanced by incorporating 1−5 wt % clay to WPUs. There are several explanations responsible for this behavior such as (i) ionic interactions between the WPU and clay may strengthen the WPU by reducing slippage during straining, (ii) the clay may act as nucleation sites to promote soft segment crystallization during straining, (iii) the clay may act as physical entanglements to reinforce tensile properties of the composites, and (iv) the clay may alter the strained microphase morphology of the WPU in such a way that results in improved tensile properties.[26]

Ionic Conductivities of the WPU/Clay Films. The volumetric and surface electrical resistances of the WPU/clay films with different clay contents are shown in Figure 12. The ionic conductivity of the WPU/clay film is mainly contributed by the ammonium carboxylate group ($COO^-NH^+(C_2H_5)_3$) of neutralized DMPA and both cations and anions of the exfoliated clay platelets. Given the fact that all these films contain a constant DMPA content, the decreases of volumetric and surface electrical resistances of the film are due to the increase of clay content. As stated quantitatively, the volumetric resistances of the WPU/clay films with clay contents of 1 and 5 wt % are 1.5×10^{11} and 3.6×10^{10} Ω·cm (corresponding surface resistances are 1.7×10^{11} and 3.2×10^{10} Ω/cm^2), respectively. Moreover, the two kinds of electrical resistances of a film are nearly identical. This indicates that clay platelets do not migrate to the surface region of the WPU/clay film because of the strong ionic interactions between the clay and WPU. On the contrary, the conventional fillers often migrate to the surface regions of their composites. The film with a surface resistance of 10^8−10^{11} Ω/cm^2 would exhibit sufficient antistatic properties.[42,43] Therefore, the WPU/clay films would exhibit antistatic property when their clay contents are above 1 wt %.

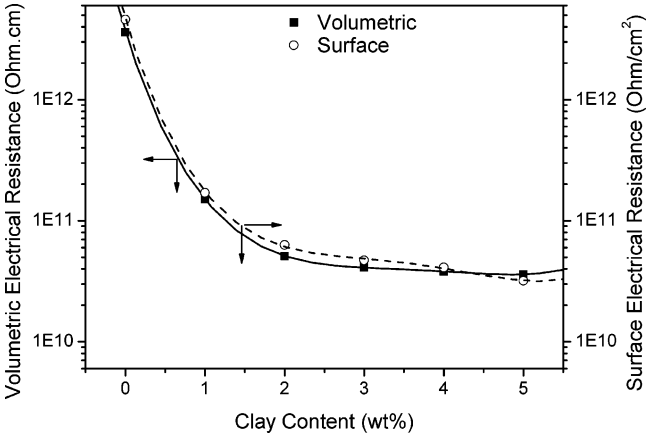

Figure 12. Volumetric and surface electrical resistances of the WPU/clay films with different clay contents.

Conclusions

Aqueous PU/clay nanocomposite dispersions were prepared through the prepolymer mixing process, while no volatile organic solvents were used. AFM phase image of the WPU/clay film shows that the isolated clay-rich phases are surrounded by a continuous WPU-rich phase. Clay does not influence T_g of the soft segment domains but raises that of the hard segment domains because of the ionic interactions between the clay and WPU hard segments. These ionic interactions could be evidenced by IR spectra of the WPU/clay nanocomposites. The WPU/clay dispersion with higher clay content exhibits a broader particle size distribution, a larger average particle size, a less negative zeta potential, and a higher viscosity. Moreover, the WPU/clay film containing more clay possesses lower volumetric and surface electrical resistances. The volumetric and surface electrical resistances of the WPU/clay nanocomposite film are nearly identical. This indicates that clay platelets do not migrate to the surface regions of WPU/clay films because of the above-mentioned ionic interactions. Clay also enhances the thermal resistance and tensile properties of WPUs substantially.

Acknowledgment. We thank the National Science Council of ROC for financial aid through Project NSC 92-2622-E238-007-CC3.

References and Notes

(1) Park, H. B.; Lee, Y. M. *J. Membr. Sci.* **2002**, *197*, 283−296.

(2) Abraham, G. A.; de Queiroz, A. A. A.; Román, J. S. *Biomaterials* **2001**, *22*, 1971−1985.
(3) Gugliuzza, A.; Clarizia, G.; Golemme, G.; Drioli, E. *Eur. Polym. J.* **2002**, *38*, 235−242.
(4) Tien, Y. I.; Wei, K. H. *Polymer* **2001**, *42*, 3213−3221.
(5) Mequanint, K.; Sanderson, R. *Polymer* **2003**, *44*, 2631−2639.
(6) Modesti, M.; Lorenzetti, A. *Eur. Polym. J.* **2001**, *37*, 949−954.
(7) Hwang, J. J.; Liu, H. J. *Macromolecules* **2002**, *35*, 7314−7319.
(8) Gorrasi, G.; Tortora, M.; Vittoria, V. *J. Polym. Sci., Part B: Polym. Phys.* **2005**, *43*, 2454−2467.
(9) Devaux, E.; Rochery, M.; Bourbigot, S. *Fire Mater*. **2002**, *26*, 149−154.
(10) Kim, D. S.; Kim, J. T.; Woo, W. B. *J. Appl. Polym. Sci.* **2005**, *96*, 164−1647.
(11) Solarski, S.; Benali, S.; Rochery, M.; Devaux, E.; Alexandre, M.; Monteverde, F.; Dubois, P. *J. Appl. Polym. Sci.* **2005**, *95*, 238−244.
(12) Ni, P.; Li, J.; Suo, J.; Li, S. *J. Appl. Polym. Sci.* **2004**, *94*, 534−541.
(13) Palau, A. M. T.; Garcia, J. C. F.; Barcelo, A. C. O.; Martinez, J. M. M. *Int. J. Adhes. Adhes.* **2001**, *21*, 1−9.
(14) Beloqui, B. J.; Garcia, J. C. F.; Barcelo, A. C. O.; Bujanda, M. M. M.; Martinez, J. M. M. *Int. J. Adhes. Adhes.* **1999**, *19*, 321−328.
(15) Goda, H.; Frank, C. W. *Chem. Mater.* **2001**, *13*, 2783−2787.
(16) Tortora, M.; Gorrasi, G.; Vittoria, V.; Galli, G.; Ritrovati, S.; Chiellini, E. *Polymer* **2002**, *43*, 6147−6157.
(17) Yao, K. J.; Song, M.; Hourston, D. J.; Luo, D. Z. *Polymer* **2002**, *43*, 1017−1020.
(18) Ma, J.; Zhang, S.; Qi, Z. *J. Appl. Polym. Sci.* **2001**, *82*, 1444−1448.
(19) Chang, J. H.; An, Y. U. *J. Polym. Sci., Part B: Polym. Phys.* **2002**, *40*, 670−677.
(20) Xu, R.; Manias, E.; Snyder, A. J.; Runt, J. *Macromolecules* **2001**, *34*, 337−339.
(21) Osman, M. A.; Mittal, V.; Morbidelli, M.; Suter, U. W. *Macromolecules* **2003**, *36*, 9851−9858.
(22) Chen, T. K.; Tien, Y. I.; Wei, K. H. *Polymer* **2000**, *41*, 1345−1353.
(23) Chen, T. K.; Tien, Y. I.; Wei, K. H. *J. Polym. Sci., Part A: Polym. Chem.* **1999**, *37*, 2225−2233.
(24) Nunes, R. C. R.; Pereira, R. A.; Fonseca, J. L. C.; Pereira, M. R. *Polym. Test.* **2001**, *20*, 707−712.
(25) Petrovic, Z. S.; Javni, I.; Waddon, A.; Banhegyi, G. *J. Appl. Polym. Sci.* **2000**, *76*, 133−151.
(26) Finnigan, B.; Jack, K.; Campbell, K.; Halley, P.; Truss, R.; Casey, P.; Cookson, D.; King, S.; Martin, D. *Macromolecules* **2005**, *38*, 7386-7396.
(27) Song, M.; Xia, H. S.; Yao, K. J.; Hourston, D. J. *Eur. Polym. J.* **2005**, *41*, 259−266.
(28) Moon, S. Y.; Kim, J. K.; Nah, C.; Lee, Y. S. *Eur. Polym. J.* **2004**, *40*, 1615−1621.
(29) Kuan, H. C.; Ma, C. C. M.; Chuang, W. P.; Su, H. Y. *J. Polym. Sci., Part B: Polym. Phys.* **2005**, *43*, 1−12.
(30) Varghese, S.; Gatos, K. G.; Apostolov, A. A.; Kocsis, J. K. *J. Appl. Polym. Sci.* **2004**, *92*, 543−551.
(31) Oertel, G. *Polyurethane Handbook*, 2nd ed.; Hanser: Munich, 1994; Chapter 2, p 29.
(32) Kim, B. K.; Seo, J. W.; Jeong, H. M. *Eur. Polym. J.* **2003**, *39*, 85−91.
(33) Hutchison, J. C.; Bissessur, R.; Shriver, D. F. *Chem. Mater.* **1996**, *8*, 1597−1599.
(34) Yano, K.; Usuki, A.; Okada, A. *J. Polym. Sci., Part A: Polym. Chem.* **1997**, *35*, 2289−2294.
(35) Malec, E. J.; David, D. J. In *Analytical Chemistry of Polyurethane*; David, D. J., Staley, H. B., Eds.; Wiley: New York, 1969; p 86.
(36) Tien, Y. I.; Wei, K. H. *Macromolecules* **2001**, *34*, 9045−9052.
(37) Socrates, G. *Infrared Characteristic Group Frequencies*; John Wiley & Sons: London, 1980; Chapter 10, p 57.
(38) Potter, E. C. *Electrochemistry*; Cleaver-Hume: London, 1970; Chapter VII, p 177.
(39) Wang, W. J.; Chin, W. K.; Wang, W. J. *J. Polym. Sci., Part B: Polym. Phys.* **2002**, *40*, 1690−1703.
(40) Nielsen, L. E. *Mechanical Properties of Polymers and Composites*; Marcel Dekker: New York, 1974; Chapter 4, p 222.
(41) Morgan, R. J.; Nielsen, L. E.; Buchdahl, R. *J. Appl. Phys.* **1971**, *42*, 4653−4659.
(42) Kim, H. K.; Kim, Y. B.; Cho, J. D.; Hong, J. W. *Prog. Org. Coat.* **2003**, *48*, 34−42.
(43) Wouters, M. E. L.; Wolfs, D. P.; van der Linde, M. C.; Hovens, J. H. P.; Tinnemans, A. H. A. *Prog. Org. Coat.* **2004**, *51*, 312−320.

MA060621Y